THE JOURNAL OF PHYSICAL CHEMISTRY A

Article

pubs.acs.org/JPCA

Production and Photodissociation of the Methyl Perthiyl Radical

Neil C. Cole-Filipiak,[†,‡,#] Mark Shapero,[†,‡] Courtney Haibach-Morris,[‡] and Daniel M. Neumark*[,†,‡]

[†]Chemical Sciences Division, Lawrence Berkeley National Laboratory, Berkeley, California 94720, United States

[‡]Department of Chemistry, University of California, Berkeley, California 94720, United States

Supporting Information

ABSTRACT: The photodissociation dynamics of the methyl perthiyl (CH_3SS) radical are investigated via molecular beam photofragment translational spectroscopy, using "soft" electron ionization to detect the radicals and their photofragments. With this new capability, we have shown that CH_3SS can be generated from flash pyrolysis of dimethyl trisulfide. Utilizing this source of radicals and the advantages afforded by soft electron ionization, we have reinvestigated the photodissociation dynamics of CH_3SS at 248 nm, finding CH_3S + S to be the dominant dissociation channel with CH_3 + SS as a minor process. These results differ from previous work reported in our laboratory in which we found CH_3 + SS and CH_2S + SH as the main dissociation channels. The difference in results is discussed in light of our new capabilities for characterization of radical production.

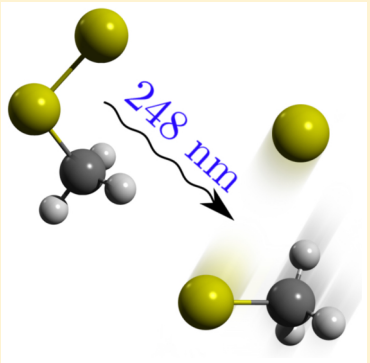

I. INTRODUCTION

Polysulfides and the sulfur-centered radicals resulting from their decomposition occur in diverse fields of chemistry. Low-valence sulfur compounds play important roles in sulfur cycle chemistry,[1,2] in proteins as the amino acid cysteine,[3] and the Venusian atmosphere.[4] Due to the prevalence of the disulfide bond in particular, alkyl disulfides have been studied extensively, with recent investigations focusing on the dynamics of alkyl disulfide photodissociation.[5−10] Dimethyl disulfide (DMDS) is known to undergo two main dissociation pathways, cleaving either the C−S or S−S bond.[5,11−13] Although the photochemistry of the thiomethoxy radical (CH_3S) has been studied,[14−16] the methyl perthiyl radical (CH_3SS) has received less attention. Apart from roles the methyl perthiyl radical may play in disulfide chemistry, the radical is of additional interest as an isovalent analog to the methyl peroxy radical (CH_3OO), an important species in combustion and atmospheric chemistry.[17−19] In this work, we investigate the ultraviolet photodissociation of CH_3SS with improved experimental capabilities compared to an earlier report from our laboratory,[20] finding markedly different results.

The electronic ground state of the methyl perthiyl radical is the $\tilde{X}^2A''$ state, in which the radical electron is delocalized over the two S atoms in a π^*-like orbital.[21,22] The ultraviolet (UV) absorption spectrum of CH_3SS has not been experimentally characterized, though spectra of HS_2 and *tert*-butyl perthiyl radicals have been measured to ∼320 nm with intensity maxima around 340−370 nm.[23,24] Ionization energies and electron affinities of the methyl perthiyl radical have been characterized experimentally[25−28] and theoretically.[22,26,29−31]

The three lowest energy dissociation channels for the methyl perthiyl radical are

$$CH_3SS(\tilde{X}^2A'') \rightarrow CH_3(\tilde{X}^2A_2'') + SS(X^3\Sigma_g^-)$$
$$D_0 = 48.6\ \text{kcal/mol} \quad (1)$$

See references 26, 32, and 33.

$$CH_3SS(\tilde{X}^2A'') \rightarrow CH_3S(\tilde{X}^2E) + S(^3P)$$
$$D_0 = 79.5\ \text{kcal/mol} \quad (2)$$

See references 15, 26, and 34.

$$CH_3SS(\tilde{X}^2A'') \rightarrow CH_2S(\tilde{X}^1A_1) + SH(X^2\Pi)$$
$$D_0 = 46\ \text{kcal/mol} \quad (3)$$

See references 26 and 29.

The CH_3 + SS channel has been observed to occur from vibrationally hot CH_3SS produced by the photodissociation of dimethyl disulfide at 193 nm.[5,11−13] Though the SH loss channel is lower in energy, the minimum energy pathway on the electronic ground state for this channel involves passage over a 50 kcal/mol isomerization barrier en route to the CH_2SSH well.[29] An S_2 loss pathway has been observed in the photodissociation of the *tert*-butyl perthiyl radical at 365 nm using EPR spectroscopy in a hydrocarbon matrix.[35]

Recent theoretical work has explored electronic excitation of the methyl perthiyl radical,[22] finding two doublet states at 1.176 eV ($1^2A'$) and 3.422 eV ($2^2A''$) above the ground state. A

Special Issue: Piergiorgio Casavecchia and Antonio Lagana Festschrift

Received: December 15, 2015
Revised: February 6, 2016

DOI: 10.1021/acs.jpca.5b12284
J. Phys. Chem. A XXXX, XXX, XXX−XXX

bound quartet state ($1^4A''$) was also found at 4.216 eV with dramatic elongation of the S−S bond. An additional $^4A'$ state was found to be repulsive along the S−S coordinate resulting in CH_3S + S, but no excitation energy to this state was given.

Our laboratory reported the first investigation of the primary photochemistry of the methyl perthiyl radical.[20] In that work, we attempted to generate CH_3SS by flash pyrolysis of DMDS, photodissociate the radical at 248 nm, and characterize the products with photofragment translational spectroscopy.[36] The results indicated both CH_3 loss (channel 1) and SH loss (channel 3); there was no evidence for S−S cleavage, the only photodissociation channel for DMDS at 248 nm.[12,13] Analysis was hindered by substantial radical precursor contamination and a lack of momentum-matched photofragment pairs from either dissociation channel. These concerns prompted our group to probe the radical photochemistry starting from the methyl perthiyl anion[37] using our fast radical beam (FRBM) photodissociation instrument,[38,39] a technique that allows for mass selection of the desired anion prior to photodetachment and photodissociation. That investigation revealed a very different methyl perthiyl photochemistry than our initial report: S atom loss, channel 2, was the dominant dissociation pathway with CH_3 loss as a minor contribution.

This discrepancy has led us to reinvestigate the photodissociation of methyl perthiyl via flash pyrolysis and photofragment translational spectroscopy. Using a different radical precursor, dimethyl trisulfide, and a newly installed tunable energy electron ionizer,[40] we were able to optimize conditions for CH_3SS production and determine its primary photochemistry at 248 nm. The results show the dominant channel to be CH_3S + S, with evidence for a small amount of CH_3 + SS production.

II. EXPERIMENTAL SECTION

The experiments described herein were performed on a universal crossed molecular beam machine with a fixed-source and rotatable detector, modified to perform photofragment translational spectroscopy; further details may be found elsewhere.[41,42] Room temperature dimethyl trisulfide (DMTS, $CH_3S_3CH_3$) was seeded in 1.2 bar of 10% N_2 in He, resulting in ∼1% DMTS. The resulting gas mixture passed through a piezoelectric pulsed valve and then through a resistively heated SiC flash pyrolysis source into the source vacuum chamber, resulting in a supersonic expansion. The pyrolysis source is based on the design of Kohn et al.[43] and has been used previously in our lab to successfully produce several radical species.[40,44,45] Power dissipated by the source is controlled by a current regulated power supply. DMTS was chosen as a radical precursor because, for alkyl sulfides with more than two sulfur atoms, the S−S bond is expected to have a dissociation energy of approximately 34 kcal/mol, ∼20 kcal/mol weaker than the C−S bond in DMTS (and DMDS, the radical precursor used in our previous work).[46] Previous work in our laboratory on the phenyl radical[45] has shown that the 10% N_2/He gas mixture results in better cooling in the flash pyrolysis source than pure He.

The free jet emerging from the source passed through two skimmers that serve to separate the source and scattering chambers and to form a collimated molecular beam in the scattering chamber. The radical beam was crossed at 90° with the 2 × 8 mm^2 focused output of a Lambda Physik LPX 220*i* excimer laser at 248 nm; typical pulse energies were 60 mJ/pulse, resulting in a photon fluence of 375 mJ cm^{-2}. Pulse energies were also varied to perform photon fluence dependence studies as discussed in the Supporting Information. The laser and pulsed valve were operated at 200 and 400 Hz, respectively, to enable isolation of the photodissociation signal via background subtraction.

Photofragments were collected as a function of the laboratory scattering angle, Θ_{lab}, relative to the molecular beam in the scattering plane defined by the molecular and laser beams. Upon entering the detector, photofragments were ionized using a "soft" electron ionization (EI) source[47] capable of producing electrons with tunable energy as low as 7 eV. Soft ionization has been shown by Casavecchia and co-workers[48] to be a powerful tool in reactive scattering experiments, because it reduces dissociative ionization (DI) in the ionizer and, as discussed below, provides a useful means for optimizing radical production.

Cations produced in the ionizer were mass-selected using a quadrupole mass filter and detected with a Daly style ion counter.[49] Ion counts were recorded and binned as a function of time relative to the laser pulse interacting with the molecular beam. The resulting time-of-flight (TOF) spectra were collected using a multichannel scaler interfaced to a computer and were typically averaged over 10^5−10^6 laser shots. All photofragment TOF spectra were simulated using an iterative forward convolution program, producing center-of-mass translational energy distributions as discussed in section IV.

The radical beam was characterized by a spinning, slotted chopper wheel. Typical beam velocities were around 1800 m/s with speed ratios, defined as the ratio of beam velocity to the spread in velocities, of ∼5. Further characterization was performed by acquiring on-axis (Θ_{lab} = 0°) mass spectra at a variety of pyrolysis source powers and monitoring depletion of the precursor parent signal at m/z = 126 ($C_2H_6S_3^+$). For selected pyrolysis source powers, appearance energy measurements were carried out for several m/z values by taking ionization efficiency curves (IECs), in which ion signal intensity was recorded as a function of electron energy for fixed electron emission current. The linear portion of the resulting curve may then be extrapolated to zero intensity, yielding the appearance energy of each ion mass. Appearance energies were used to find pyrolysis source conditions under which the $CH_3S_2^+$ signal at m/z = 79 originated from ionization of CH_3SS as opposed to DI of the DMTS precursor.

To determine the photofragment angular distribution, laser polarization studies were performed by passing the unpolarized excimer laser light through a stack of eight quartz plates at Brewster's angle. The stack was held in a rotatable mount, allowing for rotation of the electric field with respect to the plane defined by the molecular beam and detector axis. The laser polarization was rotated while monitoring photodissociation signal at fixed laboratory scattering angle, similar to the work described by Butler and co-workers.[50,51] The polarization purity was determined by passing the output from the quartz stack through a birefringent MgF_2 prism, resulting in two spatially separated, linearly polarized spots. Measuring the intensity of each spot indicated that the combined output from the quartz stack is a 9:1 mixture of the two linear polarizations.

Pyrolysis and photodissociation experiments were also performed under the conditions of our previous study in which DMDS was used as the radical precursor[20] and on the photodissociation of DMTS itself; details of these experiments may be found in the Supporting Information.

DOI: 10.1021/acs.jpca.5b12284
J. Phys. Chem. A XXXX, XXX, XXX−XXX

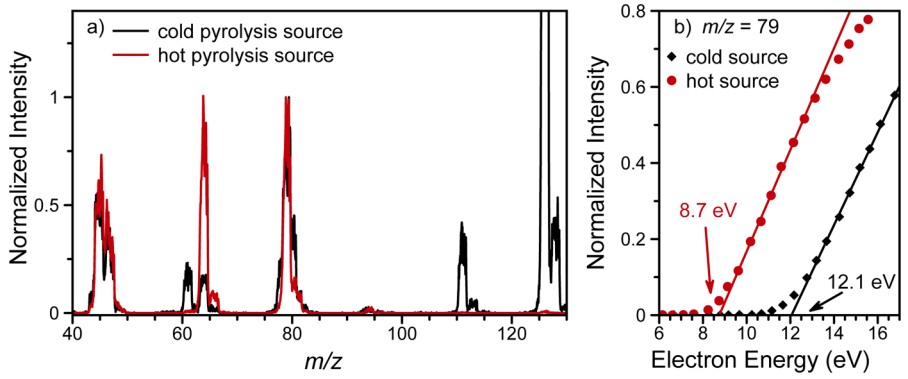

Figure 1. (a) Mass spectra of the molecular beam taken at two different pyrolysis source powers normalized to the signal at m/z = 79. The black trace (cold pyrolysis source) shows the precursor mass spectrum using an electron ionization energy of 19 eV. The red trace (hot pyrolysis source) shows depletion of the precursor peak. (b) Ionization efficiency curves for the m/z = 79 component of the molecular beam with the pyrolysis source cold (black) and hot (red).

III. RESULTS

Figure 1a shows mass spectra of the molecular beam at two different pyrolysis source conditions: a "cold" pyrolysis source (dissipating 0 W), and a "hot" pyrolysis source (dissipating 45 W). As the power dissipated by the source is increased, the DMTS parent peak at m/z = 126 disappears, leaving peaks at m/z = 79 ($CH_3S_2^+$), 64 (S_2^+), and 47 (CH_3S^+). Under a third set of conditions at even higher power (80 W), termed "very hot", the m/z = 79 contribution in the molecular beam is depleted, leaving a dominant feature at m/z = 64. Though the source temperature was not directly measured, consistent source temperatures were assumed as the power dissipated by the source was held constant for each set of conditions.

Figure 1b shows the IECs at m/z = 79 under cold and hot pyrolysis source conditions. An appearance energy of 12.1 eV at m/z = 79 was found with the cold source, in agreement with the previously reported[52] value of 12.3 ± 0.3 eV for the appearance of CH_3SS^+ from DMTS. With a hot pyrolysis source, the curve visibly shifts and the appearance energy decreases to 8.7 eV, in good agreement with the known ionization energy of 8.63 eV for CH_3SS.[28] Similarly, m/z = 47 shows an appearance energy of 12.5 eV with a cold pyrolysis source (previously reported[52] as 12.9 ± 0.2 eV), dropping to 9.2 eV with a hot pyrolysis source, consistent with the production of CH_3S.[53] It is important to note that, for dissociative ionization, an appearance energy derived from a linear extrapolation is not equivalent to the thermochemical threshold for daughter ion formation.[54] A more rigorous fit of the threshold region using a power law, as discussed in detail elsewhere,[55] yields dissociative ionization thresholds of 10.6 ± 0.6 and 10.4 eV ± 0.6 eV, respectively, in excellent agreement with the expected values of 10.8 eV for $CH_3S^+ + CH_3SS$ and 10.1 eV for $CH_3S + CH_3SS^+$ from DMTS.[28,46,56] Similar measurements were performed with the DMDS precursor as discussed in the Supporting Information. Unlike DMTS, pyrolysis of DMDS appears to only produce small quantities of CH_3SS before decomposing to S_2.

TOF spectra were taken for photofragment signals at m/z = 79, 64, 47, 46 (CH_2S^+), 45 (CHS^+), 44 (CS^+), 33 (SH^+), 32 (S^+), and 15 (CH_3^+), accounting for the dissociation channels 1−3 and daughter ions from dissociative ionization (DI) during EI. With a cold pyrolysis source, DMTS photodissociation using an electron ionization energy of 16 eV revealed one TOF feature at m/z = 79 and 47; further discussion may be found in the Supporting Information. With a hot pyrolysis source, no photodissociation signal was observed at m/z = 79 for spectra averaged for 10^6 laser shots, consistent with total depletion of the DMTS under these conditions.

Sample TOF spectra taken with a hot pyrolysis source and an electron ionization energy of 19 eV are shown in Figures 2 and 3. Figure 2 shows TOF spectra at m/z = 47 at Θ_{lab} = 15° and 40°. These spectra exhibit one sharp peak; similar spectra are seen from Θ_{lab} = 15−45°. TOF spectra at m/z = 47 and Θ_{lab} < 15° exhibit an additional slow peak. Figure 2 also shows TOF spectra at m/z = 32 at Θ_{lab} = 15° and 25°; the two features seen here persist out to Θ_{lab} = 45°, the highest angle taken at this m/z value. TOF spectra taken at m/z = 32 and high electron energy (100 eV) do not have well resolved features, most likely due to ionization of background O_2; example spectra are shown in the Supporting Information. TOF spectral features at m/z = 46 and 45, as well as the second TOF feature at m/z = 32 and 47, are attributed to CH_3S photodissociation and are discussed in the Supporting Information. Spectra at m/z = 33 comprise several overlapping, unresolved features.

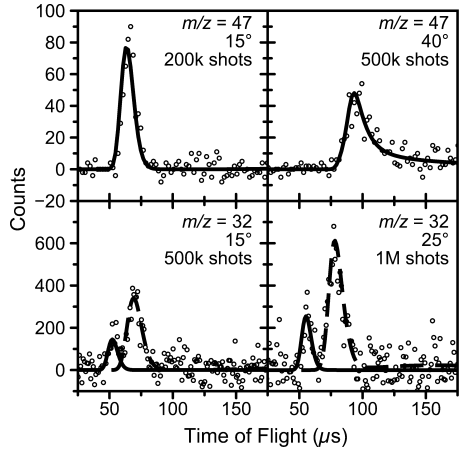

Figure 2. Example TOF spectra taken at m/z = 47 (top row, 2 μs bin width) and m/z = 32 (bottom row, 1 μs bin width) using unpolarized laser light and an electron ionization energy of 19 eV. The open circles are data, and the solid line is a forward convolution simulation from the $P(E_T)$ in Figure 5. The dashed lines at m/z = 32 are a forward convolution simulation from the $P(E_T)$ in Figure S9 assuming CH_3S photodissociation.

DOI: 10.1021/acs.jpca.5b12284
J. Phys. Chem. A XXXX, XXX, XXX−XXX

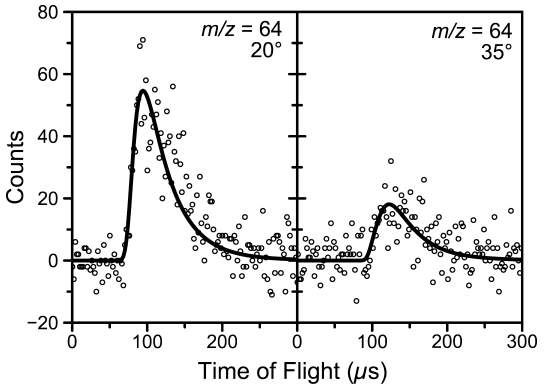

Figure 3. Example TOF spectra taken at m/z = 64 using unpolarized laser light and an electron ionization energy of 19 eV. The open circles are data, and the solid line is a forward convolution simulation from the $P(E_T)$ in Figure 6.

The TOF spectra in Figure 3 show one broad feature at m/z = 64 at Θ_{lab} = 20° and 35°, observed over Θ_{lab} = 5°−35° that could arise from dissociation of CH_3SS to CH_3 + SS. The only TOF feature found at m/z = 15 appears to be DI of the fast feature at m/z = 47. Owing to unfavorable kinematics and either high background signal (due to large background gas DI at high electron ionization energies) or a low EI cross section at low electron ionization energies,[57] no CH_3 photofragment signal from CH_3 + SS is observed. TOF spectra were also taken using the very hot pyrolysis source conditions that deplete CH_3SS from the molecular beam. Multiple photodissociation features present with the hot source were absent with a very hot source; representative spectra may be found in Figure S12.

Figure 4 shows the results of the laser polarization study for m/z = 47 photoproduct at Θ_{lab} = 15° and the m/z = 64 photoproduct at Θ_{lab} = 20°. To determine the signal intensity, the entire m/z = 47 TOF spectrum was integrated while, at m/z = 64, a 50 μs window centered at the peak was integrated. These signals are plotted as a function of φ, the angle between the laser polarization and the scattering plane. At m/z = 47, a clear drop in photofragment intensity is observed as φ increases from 0° to 90°. Conversely, the intensity at m/z = 64 appears to have no dependence upon the laser polarization angle.

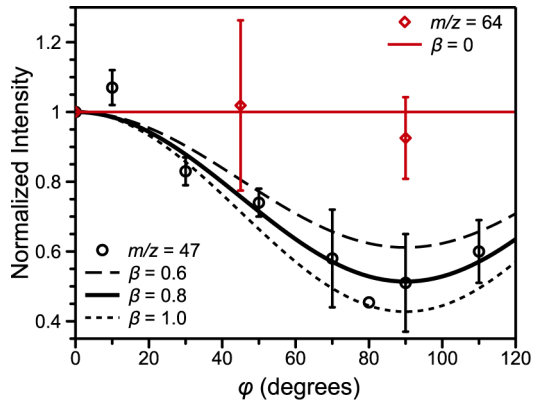

Figure 4. Photofragment intensity at m/z = 47 (black) and m/z = 64 (red) as a function of φ. Intensities are normalized to φ = 0°, the lowest angle recorded. Error bars represent the standard deviation from the average intensity for repeated values of φ. The curves are plots of eq 6 for the indicated values of β, also normalized to φ = 0°.

The attempt to replicate previous experimental results using DMDS as the radical precursor is found in the Supporting Information. Briefly, a pyrolysis source dependent photodissociation feature at m/z = 64 is again observed, along with a feature at m/z = 79 and m/z = 47, 46, and 45. Very low energy electron ionization mass spectra and appearance energy measurements of molecular beam constituents taken at a variety of pyrolysis source powers show little to no production of CH_3SS from DMDS.

IV. ANALYSIS

Taken together, the results presented above strongly indicate that DMTS is pyrolyzed under hot source conditions to produce the methyl perthiyl radical and that we observe clear photodissociation signal under these source conditions. To analyze these laboratory-frame data, we determine the corresponding center-of-mass translational energy and angular distributions $P(E_T,\theta)$. These distributions are generated by simulating the observed TOF features assuming uncoupled center-of-mass translational and angular distributions,

$$P(E_T,\theta) = P(E_T)\, I(\theta) \tag{4}$$

where $P(E_T)$ is the CM translational energy distribution and $I(\theta)$ is the photofragment angular distribution. The photofragment intensity dependence on the laser polarization in center-of-mass coordinates has the functional form:[58]

$$I(\theta) = \frac{1}{4\pi}[1 + \beta P_2(\cos\theta)] \tag{5}$$

where β is the anisotropy parameter, $P_2(x)$ is the second degree Legendre polynomial, and θ is the CM scattering angle (the angle between the electric field vector and the CM product recoil axis). The anisotropy parameter ranges in value from +2 to −1 depending on whether the transition dipole is parallel or perpendicular to the dissociation axis.

For incomplete polarization of the laser light, the observed TOF intensities will have contributions from both linear polarizations and eq 5 must be rewritten to account for the incomplete polarization. For the experimental geometry used herein, eq 5 becomes

$$I(\theta) \propto \frac{3}{2}\beta(\cos^2\omega)[x\cos^2\varphi + (1-x)\sin^2\varphi] \tag{6}$$

where ω is the angle between the CM recoil axis and the molecular beam in the scattering plane, φ is the angle between the electric field vector and the scattering plane, $\cos\theta = \cos\omega\cos\varphi$, and x is the dominant fraction of light polarization (x = 0.9 for this experiment). To determine ω, the TOF signal at each m/z value was assumed to come from a single CM velocity corresponding to the peak of the TOF spectrum, yielding ω = 35° at m/z = 47 and 68° at m/z = 64. The value of β may be determined by plotting eq 6 along with photofragment intensity for fixed laboratory scattering angle versus φ, as shown in Figure 4 for the m/z = 47 photofragment at Θ_{lab} = 15° and m/z = 64 photofragment at Θ_{lab} = 20°.[50] The best overall agreement between the CH_3S TOF intensity data and eq 6 appears to be for β = 0.8. To estimate the error in the anisotropy parameter, eq 6 was plotted for several values of β that still simulated the experimental data, yielding β = 0.8 ± 0.2. The m/z = 64 intensity data shown in Figure 4 have no clear dependence on the laser polarization, suggesting an isotropic angular distribution.

DOI: 10.1021/acs.jpca.5b12284
J. Phys. Chem. A XXXX, XXX, XXX−XXX

The PHOTRAN forward convolution program[59] is used to produce the CM translational energy distributions shown in Figures 5 and 6. Trial forms of the distribution are iteratively

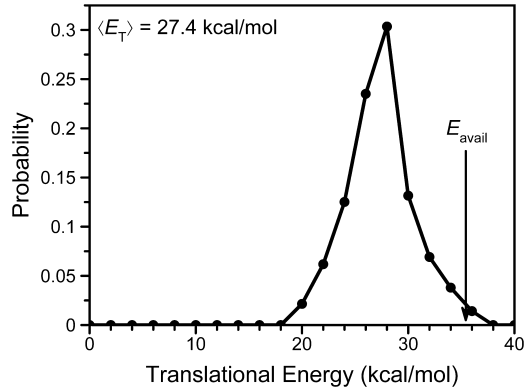

Figure 5. Center-of-mass $P(E_T)$ assuming anisotropic S−S bond fission (β = 0.8) from the methyl perthiyl radical used to simulate the TOF spectra in Figure 2 (solid line). The maximum observed translational energy is 38 kcal/mol.

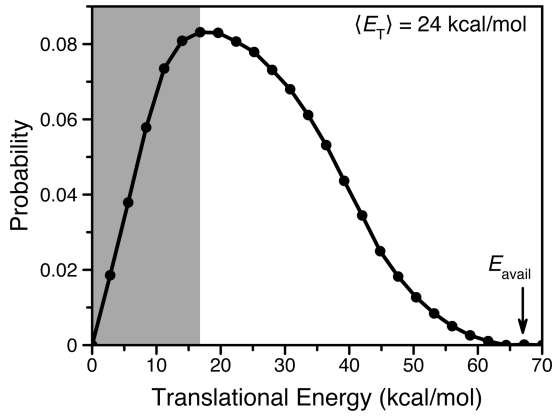

Figure 6. Center-of-mass $P(E_T)$ assuming isotropic C−S bond fission from the methyl perthiyl radical used to simulate the TOF spectra in Figure 3. The maximum translational energy is 67 kcal/mol in agreement with the expected E_{avail} = 66 kcal/mol. Translational energies below ∼17 kcal/mol (shaded gray) are uncertain due to a slower contribution to the photodissociation feature appearing at lower laboratory scattering angles and m/z = 64.

adjusted point-wise until TOF simulations agree with all photofragment data for all scattering angles acquired with unpolarized laser light. For the CH_3S + S distribution in Figure 5, a value of β = 0.8 was used whereas the CH_3 + SS $P(E_T)$ shown in Figure 6 was produced using an isotropic (β = 0) angular distribution.

By conservation of energy, the available energy (E_{avail}) in photodissociation is given by

$$E_{avail} = h\nu - D_0 + E_0 = E_T + E_{int} \quad (7)$$

where $h\nu$ is the photon energy, D_0 is the bond dissociation energy, E_0 is the nascent radical internal energy, E_T is the photoproduct translational energy, and E_{int} is the photoproduct internal energy. In the limit of internally cold radicals (E_0 = 0) and photoproducts (E_{int} = 0), the maximum translational energy is given by $E_{avail} = h\nu - D_0 = E_T$.

The simulations shown in Figure 2 were generated using the translational energy distribution shown in Figure 5. The distribution peaks at 28 kcal/mol with an average translational energy ⟨E_T⟩ = 27.4 kcal/mol and extends to 38 kcal/mol. A key feature of the TOF assignments is that counterfragments from a dissociation channel must be described by the same translational energy distribution. As shown in Figure 2, the fast features at m/z = 47 and m/z = 32 can be simulated as "momentum-matched" CH_3S and S fragments from CH_3SS dissociation. Further evidence of the assignment is the agreement between the observed maximum translational energy and the expected E_{avail}.

Assignment of the m/z = 64 TOF spectra of Figure 3 is not as straightforward. Without evidence for the CH_3 counter fragment, the observed feature can only be tentatively assigned to the CH_3 + SS product channel. Caution is required as spectra for $\Theta_{lab} \leq 15°$ show an increasingly prominent contribution at longer flight times (see Figure S13 in the Supporting Information for an example of the TOF spectrum) that persists under the very hot pyrolysis source conditions that deplete CH_3SS from the molecular beam. Although this contribution to the TOF does not appear to be from the methyl perthiyl radical, it obscures signal from CH_3SS at long flight times. The TOF data for $\Theta_{lab} \geq 20°$ in Figure 3 were simulated with the $P(E_T)$ shown in Figure 6. This distribution has an average translational energy ⟨E_T⟩ = 24 kcal/mol, peaks around 17 kcal/mol, and extends to the expected E_{avail}. Attempts to simulate the slower contribution assuming methyl perithyl photodissociation were unsuccessful, consistent with the interpretation that this TOF contribution is not from CH_3SS.

For the TOF features currently attributed to CH_3SS photodissociation, other sources of signal must be considered, as DMTS pyrolyzes not only to methyl perthiyl radical but also to CH_3S (by necessity) and possibly S_2 (based our results with a very hot source). Either of these may absorb a photon at 248 nm[60,61] and CH_3S photodissociation does appear to contribute to some of the observed TOF signal, but neither can account for all of the observed photodissociation features. Small amounts of DMDS are present in our DMTS sample, but the observed TOF features are not consistent with DMDS photodissociation at 248 nm.[13,20] CS_2 and S_3 appear as minor contributions in the mass spectrum in Figure 1 with the pyrolysis source on. CS_2 does not absorb 248 nm light,[62,63] and there was no evidence for the momentum-matched m/z = 32 counter fragment assuming that S_3 dissociation produces the features at m/z = 64. As such, the most reasonable conclusion is that the methyl perthiyl radical photodissociates via the CH_3S + S and CH_3 + SS pathways.

We next consider the branching ratio for these two channels. In previous work in our lab, most recently on the benzyl radical,[40] product branching ratios were determined by finding at least one m/z value with TOF contributions from all photoproduct channels. Here, however, no single m/z value shows features from both CH_3SS dissociation pathways. Nonetheless, the photodissociation product channel branching ratio may be calculated using the following equation:[64]

$$\frac{N_1^+(\Theta_{lab},E_{elec})}{N_3^+(\Theta_{lab},E_{elec})} \times \frac{\sigma_3(E_{elec})}{\sigma_1(E_{elec})} \times \frac{f_3(E_{elec})}{f_1(E_{elec})} \times \frac{T_3}{T_1} = BR(A/B) \times \left(\frac{m_1 \times m_4}{m_2 \times m_3}\right) \times \frac{\int P_A(E_T)\, I_A(\theta) v_1/u_1 \, dv_1}{\int P_B(E_T)\, I_B(\theta) v_3/u_3 \, dv_3} \quad (8)$$

DOI: 10.1021/acs.jpca.5b12284
J. Phys. Chem. A XXXX, XXX, XXX−XXX

The notation in eq 8 assumes two photodissociation channels, with masses $m_1 + m_2$ from channel A and $m_3 + m_4$ from channel B. For the analysis below, channel A will be CH_3S + S with m_1 = 47 amu as the detected mass and channel B will be CH_3 + SS with m_3 = 64 amu. The left side of eq 8 calculates the ratio of neutral photofragment intensities from two channels at a given laboratory scattering angle: $N_i^+(\Theta_{lab},E_{elec})$ is the laboratory TOF signal of the species of interest at Θ_{lab} and electron ionization energy E_{elec}, σ_i is the electron ionization cross section, f_i is the probability of appearing at that m/z value, and T_i is the ion transmission probability through the quadrupole. On the right side of eq 8, BR(A/B) is the product branching ratio of channel A to channel B, m_i is the mass of species i, and v_i and u_i are the laboratory and CM velocities of photofragment i, respectively. For each point in the integration, u_i and θ are determined by the velocity of the molecular beam, the photofragment laboratory velocity v_i, and the laboratory scattering angle Θ_{lab}. The molecular beam was assumed to have a uniform velocity of 1800 m/s. Each integral evaluates the probability that a CM velocity will result in a laboratory velocity that contributes to the TOF at a given Θ_{lab}. Further details and a derivation of this relationship may be found in Appendix B of ref 64.

The electron ionization cross section σ_i may be calculated using the binary-encounter-Bethe (BEB) model;[65] details of this calculation may be found in the Supporting Information. Briefly, the BEB model takes an orbital binding energy and electron kinetic energy (calculated using the Q-Chem software package[66]) to calculate an electron ionization cross section for each orbital for a given electron ionization energy. The total electron ionization cross section is then determined by summing all orbital cross sections. As the calculated cross sections showed a dependence on the theoretical method employed, all combinations of the cross section ratio in eq 8 were calculated and an average ionization cross section ratio of 1.4 ± 0.2 was found. The third term in eq 8, f_i, was determined by collecting TOF spectra at each m/z value with measurable signal; values of 44% for CH_3S at m/z = 47 and 100% for S_2 at m/z = 64 were found using an electron ionization energy of 19 eV. As the difference in m/z for the two fragments is small compared to the mass range of the radio frequency oscillator used in these experiments, the ratio of transmission probabilities is approximated as unity. The translational energy distributions shown in Figures 5 and 6 were used for $P_A(E_T)$ and $P_B(E_T)$, respectively, with β = 0.8 or 0 for the respective angular distributions. Averaging over all of the calculated cross sections and the BR determined at Θ_{lab} = 20−35°, the product branching ratio is 15(10):1 in favor of the CH_3S + S pathway. The error in the branching ratio was estimated by calculating the BR using a range of CH_3 + SS translational energy distributions that still produce reasonable simulations of the m/z = 64 TOF spectra for Θ_{lab} = 20−35°.

V. DISCUSSION

The principal objective of this study was to reconcile the differences between our previous investigation of the methyl perthiyl radical[20] with recent results from our group.[37] Our original investigation suggested dissociation via C−S bond cleavage and an apparent SH loss channel whereas the FRBM results revealed almost exclusive S−S bond fission. As mentioned above and discussed in the Supporting Information, our current results suggest that flash pyrolysis of our original precursor, dimethyl disulfide, did not produce sufficient quantities of CH_3SS to determine the radical's photochemistry. DMTS appears to be a superior precursor for CH_3SS production because S−S bond cleavage requires less energy than the C−S bond cleavage required with DMDS (see literature value comparison in section II).[46]

It is important to note that the data previously presented do not appear to be in error: replication of our previous experiment again revealed a pyrolysis source dependent TOF feature at m/z = 64 and m/z = 46. In the original investigation, TOF spectra acquired at m/z = 79 showed no discernible photofragment signal. These TOF spectra, though, were not acquired for a sufficient number of laser shots to observe the photodissociation signal at this m/z value as shown in Figure S3 in the Supporting Information—evidence that would have called into question assumption of methyl perthiyl radical photodissociation. Information about the ionization energy of species in the molecular beam was not available at the time. Thus, our primary error appears to have been the assumption of methyl perthiyl production and photodissociation. Taken with the results from our investigations of the phenyl radical,[45,67] this work again highlights the exceptional care that must be taken when one attempts to produce and study these reactive intermediates.

In the present work, analysis of the molecular beam shows good agreement between the measured and literature vales for the methyl perthiyl radical ionization energy. Photodissociation at m/z = 47 and 32 show momentum-matched photofragments with the resulting $P(E_T)$ in agreement with the most recent results from our group.[37] Disappearance of the photodissociation features attributed to the methyl perthiyl radical under the "very hot" pyrolytic conditions that remove the m/z = 79 contribution from the molecular beam strongly suggests that these photofragments are from CH_3SS. The preponderance of evidence presented herein thus indicates CH_3SS production and photodissociation and we now proceed onto our original goal of determining this radical's primary photochemistry.

For the CH_3S + S channel, the $P(E_T)$ in Figure 5 is peaked far away from zero translational energy and very close to the available energy for electronic ground state photoproducts. This type of behavior is indicative of dissociation on a repulsive electronic state.[36] This interpretation is supported by the measurable photofragment anisotropy, a signature of rapid dissociation prior to substantial energy redistribution or rotational motion of the photoexcited radical.[68] The agreement between the fastest translational energy observed in the distribution shown in Figure 5 (38 kcal/mol) and that expected on the basis of the S−S bond dissociation energy (35.5 kcal/mol) suggests that the (unknown) internal energy of the radicals produced in the flash pyrolysis source does not markedly affect the photofragment translational energy distribution.

The CH_3 + SS channel is less straightforward to assess than the S atom loss channel. The broad, unstructured translational energy distribution shown in Figure 6 is peaked away from either E_T = 0 or E_{avail} and is not consistent with dissociation on a repulsive state nor does complete vibrational energy redistribution seem to have occurred. Further dynamical information cannot be inferred without the portion of the translational energy distribution below 17 kcal/mol. Nonetheless, given that CH_3 + SS is a low energy dissociation channel, it is possible it arises from internal conversion to the ground state followed by dissociation to these products, which would be

DOI: 10.1021/acs.jpca.5b12284
J. Phys. Chem. A XXXX, XXX, XXX−XXX

consistent with the apparent isotropic angular distribution shown in Figure 4.

Although TOF spectra at m/z = 46 and m/z = 33 exhibit a photodissociation signal not attributed to S atom loss, these features remain under the very hot pyrolysis source conditions that remove CH_3SS from the molecular beam. Trial translational energy distributions assuming CH_2S + SH (channel 3) could not simultaneously simulate the observed spectral features, supporting the conclusion that these photofragments are not from the methyl perthiyl radical. Thus, our current results suggest that SH loss is at most a very minor process after photoexcitation at 248 nm.

The current CH_3SS photodissociation results are in agreement with the FRBM study[37] at 248 nm. Both experiments conclude that S atom loss occurs on a repulsive excited state to produce ground state photoproducts. The measured anisotropy parameter of 0.8 is consistent with a parallel transition and in qualitative agreement with the FRBM value of 1.4. The reported branching ratio of (S atom loss/CH_3 loss) = 15 (i.e., 94% S atom loss) is also in excellent agreement with the FRBM result of 96% S atom loss from vibrationally cold CH_3SS. Although this comparison and the translational energy distribution in Figure 5 do not directly address the internal energy distribution of the radicals produced by flash pyrolysis, always a point of concern, they do indicate that whatever internal energy is present does not substantially affect the photodissociation dynamics reported here.

VI. CONCLUSION

The photodissociation dynamics of the methyl perthiyl radical have been reinvestigated at 248 nm. With a new precursor and the ability to characterize our radical pyrolysis source with soft electron ionization, we have been able to verify CH_3SS production and photodissociation. We find clear evidence through the observation of momentum-matched photofragments that the major dissociation channel is CH_3S + S on a repulsive surface, and additional indications that CH_3 + SS occurs as a minor channel. These results are in overall agreement with recent results in our laboratory on another instrument. The work presented herein showcases the advantages of using a tunable energy electron ionizer for both radical characterization and simplification of photodissociation spectra.

■ ASSOCIATED CONTENT

Supporting Information

The Supporting Information is available free of charge on the ACS Publications website at DOI: 10.1021/acs.jpca.5b12284.

Discussion of the reproduction of the original experiment DMTS photodissociation and thiomethoxy radical photodissociation, including mass spectra, appearance energies, TOF spectra, and bond fission probability; additional results from the present investigation, including TOF spectra laser pulse energy studies, depletion of CH_3SS from the molecular beam, BEB model calculation, and total electron ionization cross sections (PDF)

■ AUTHOR INFORMATION

Corresponding Author

*D. Neumark. Electronic mail: dneumark@berkeley.edu. Telephone: +1 (510) 642-3502.

Present Address

[#]Department of Chemistry, University of Warwick, Coventry CV4 7AL, United Kingdom.

Notes

The authors declare no competing financial interest.

■ ACKNOWLEDGMENTS

The authors thank Narbe Mardirossian and Yuezhi Mao for assistance with Q-Chem, Patrick W. Smith for synthesis of a potential radical precursor, and Drs. Aaron W. Harrison and Mikhail Ryazanov for helpful discussions. This work was supported by the Director, Office of Basic Energy Sciences, Chemical Sciences, Geosciences, and Biosciences Division of the U.S. Department of Energy under Contract No. DE-AC02-05CH11231.

■ REFERENCES

(1) Graedel, T. E. The Homogeneous Chemistry of Atmospheric Sulfur. *Rev. Geophys.* **1977**, *15*, 421−428.

(2) Tyndall, G. S.; Ravishankara, A. R. Atmospheric Oxidation of Reduced Sulfur Species. *Int. J. Chem. Kinet.* **1991**, *23*, 483−527.

(3) Huxtable, R. J.; Lafranconi, W. M. *Biochemistry of Sulfur*; Plenum Press: New York, 1986.

(4) Prinn, R. G. On the Possible Roles of Gaseous Sulfur and Sulfanes in the Atmosphere of Venus. *Geophys. Res. Lett.* **1979**, *6*, 807−810.

(5) Martínez-Haya, B.; Bass, M. J.; Brouard, M.; Vallance, C.; Torres, I.; Barr, J. Photodissociation and Pultiphoton Dissociative Ionization Processes in $CH_3S_2CH_3$ at 193 nm Studied Using Velocity-Map Imaging. *J. Chem. Phys.* **2004**, *120*, 11042−11052.

(6) Rinker, A.; Halleman, C. D.; Wedlock, M. R. Photodissociation Dynamics of Dimethyl Disulfide. *Chem. Phys. Lett.* **2005**, *414*, 505−508.

(7) Luo, C.; Du, W.-N.; Duan, X.-M.; Liu, J.-Y.; Li, Z.-S. Theoretical Study on the Excited States and Photodissociation Mechanism of Dimethyldisulfide. *Chem. Phys. Lett.* **2009**, *469*, 242−246.

(8) Stephansen, A. B.; Brogaard, R. Y.; Kuhlman, T. S.; Klein, L. B.; Christensen, J. B.; Sølling, T. I. Surprising Intrinsic Photostability of the Disulfide Bridge Common in Proteins. *J. Am. Chem. Soc.* **2012**, *134*, 20279−20281.

(9) Stephansen, A. B.; Larsen, M. A. B.; Klein, L. B.; Sølling, T. I. On the Photostability of the Disulfide Bond: An Electronic or a Structural Property? *Chem. Phys.* **2014**, *442*, 77−80.

(10) Denis, P. A. Coupled Cluster Investigation on the Thermochemistry of Dimethyl Sulphide, Dimethyl Disulphide and Their Dissociation Products: The Problem of the Enthalpy of Formation of Atomic Sulphur. *Mol. Phys.* **2014**, *112*, 1167−1173.

(11) Callear, A. B.; Dickson, D. R. Transient Spectra and Primary Processes in the Flash Photolysis of CH_3SSCH_3, CH_3SCH_3, CH_3SH and C_2H_5SH. *Trans. Faraday Soc.* **1970**, *66*, 1987−1995.

(12) Nourbakhsh, S.; Liao, C. L.; Ng, C. Y. A 193 nm Laser Photofragmentation Time-of-Flight Mass Spectrometric Study of CH_3SSCH_3, $SSCH_3$, and SCH_3. *J. Chem. Phys.* **1990**, *92*, 6587−6593.

(13) Lee, Y. R.; Chiu, C. L.; Lin, S. M. Ultraviolet Photodissociation Study of CH_3SCH_3 and CH_3SSCH_3. *J. Chem. Phys.* **1994**, *100*, 7376−7384.

(14) Hsu, C.-W.; Liao, C.-L.; Ma, Z.-X.; Tjossem, P. J. H.; Ng, C. Y. A study of the $S(^3P_{2,1,0};^1D_2)$ Production in the 193 nm Photodissociation of CH3S($\tilde{X}$). *J. Chem. Phys.* **1992**, *97*, 6283−6290.

(15) Bise, R. T.; Choi, H.; Pedersen, H. B.; Mordaunt, D. H.; Neumark, D. M. Photodissociation Spectroscopy and Dynamics of the Methylthio Radical (CH_3S). *J. Chem. Phys.* **1999**, *110*, 805−816.

(16) Zheng, X.; Song, Y.; Wu, J.; Zhang, J. H-Atom Product Channel and Mode Specificity in the Near-UV Photodissociation of Thiomethoxy Radical via the $\tilde{A}^2A_1$ State. *Chem. Phys. Lett.* **2008**, *467*, 46−51.

DOI: 10.1021/acs.jpca.5b12284
J. Phys. Chem. A XXXX, XXX, XXX−XXX

(17) Lightfoot, P. D.; Cox, R. A.; Crowley, J. N.; Destriau, M.; Hayman, G. D.; Jenkin, M. E.; Moortgat, G. K.; Zabel, F. Organic Peroxy Radicals: Kinetics, Spectroscopy and Tropospheric Chemistry. *Atmos. Environ., Part A* **1992**, *26*, 1805−1961.
(18) Frost, G. J.; Ellison, G. B.; Vaida, V. Organic Peroxyl Radical Photolysis in the Near-Infrared: Effects on Tropospheric Chemistry. *J. Phys. Chem. A* **1999**, *103*, 10169−10178.
(19) Taatjes, C. A. Uncovering the Fundamental Chemistry of Alkyl + O_2 Reactions via Measurements of Product Formation. *J. Phys. Chem. A* **2006**, *110*, 4299−4312.
(20) Cole-Filipiak, N. C.; Negru, B.; Just, G. M. P.; Park, D.; Neumark, D. M. Photodissociation Dynamics of the Methyl Perthiyl Radical at 248 nm via Photofragment Translational Spectroscopy. *J. Chem. Phys.* **2013**, *138*, 054301.
(21) Hadley, J. H.; Gordy, W. Nuclear Coupling of ^{33}S and the Nature of Free Radicals in Irradiated Crystals of Cystine Dihydrochloride. *Proc. Natl. Acad. Sci. U. S. A.* **1974**, *71*, 3106−3110.
(22) Song, M.-X.; Zhao, Z.-X.; Zhang, W.; Bai, F.-Q.; Zhang, H.-X.; Sun, C.-C. A CASSCF/CASPT2 Study on the Low-Lying Electronic States of the CH_3SS and Its Cation. *Int. J. Quantum Chem.* **2012**, *112*, 1537−1546.
(23) Porter, G. The Absorption Spectroscopy of Substances of Short Life. *Discuss. Faraday Soc.* **1950**, *9*, 60−69.
(24) Burkey, T. J.; Hawari, J. A.; Lossing, F. P.; Lusztyk, J.; Sutcliffe, R.; Griller, D. The *tert*-Butylperthiyl Radical. *J. Org. Chem.* **1985**, *50*, 4966−4967.
(25) Moran, S.; Ellison, G. B. Photoelectron Spectroscopy of Sulfur Ions. *J. Phys. Chem.* **1988**, *92*, 1794−1803.
(26) Ma, Z.-X.; Liao, C. L.; Ng, C. Y.; Cheung, Y.-S.; Li, W.-K.; Baer, T. Experimental and Theoretical Studies of Isomeric CH_3S_2 and $CH_3S_2^+$. *J. Chem. Phys.* **1994**, *100*, 4870−4875.
(27) Cheng, B.-M.; Chew, E. P.; Hung, W.-C.; Eberhard, J.; Lee, Y.-P. Photoionization Studies of Sulfur Radicals and Products of Their Reactions. *J. Synchrotron Radiat.* **1998**, *5*, 1041−1043.
(28) Maofa, G.; Jing, W.; Zheng, S.; Xinjiang, Z.; Dianxun, W. First Experimental Observation on Different Ionic States of the CH_3SS Radical: A HeI Photoelectron Spectrum. *J. Chem. Phys.* **2001**, *114*, 3051−3054.
(29) Cheung, Y.-S.; Li, W.-K.; Ng, C.-Y. A Gaussian-2 *Ab Initio* Study of Isomeric CH_3S_2, $CH_3S_2^+$ and $CH_3S_2^-$. *J. Mol. Struct.: THEOCHEM* **1995**, *339*, 25−38.
(30) Krauss, M.; Roszak, S. Calculation of Disulfide Neutral and Anion Molecular Excitation Energies. *J. Phys. Chem.* **1992**, *96*, 8325−8328.
(31) Gao, A.; Du, H.; Li, A.; Pei, H. Studies on Structures and Electron Affinities of the Simplest Alkyl Dithio Radicals and Their Anions with Gaussian-3 Theory and Density Functional Theory. *J. Mol. Model.* **2013**, *19*, 2443−2449.
(32) McCulloh, K. E.; Dibeler, V. H. Enthalpy of Formation of Methyl and Methylene Radicals of Photoionization Studies of Methane and Ketene. *J. Chem. Phys.* **1976**, *64*, 4445−4450.
(33) NIST-JANAF thermochemical tables. http://kinetics.nist.gov/janaf/ (accessed December 9, 2015).
(34) Nagy, B.; Szakács, P.; Csontos, J.; Rolik, Z.; Tasi, G.; Kállay, M. High-Accuracy Theoretical Thermochemistry of Atmospherically Important Sulfur-Containing Molecules. *J. Phys. Chem. A* **2011**, *115*, 7823−7833.
(35) Mikhailik, V. V.; Razskazovskii, Y. V.; Mel'nikov, M. Y. Photochemical Reactions of Peroxide and Perthiyl Radicals at 77 K. *Dokl. Akad. Nauk* **1982**, *263*, 934.
(36) Butler, L. J.; Neumark, D. M. Photodissociation Dynamics. *J. Phys. Chem.* **1996**, *100*, 12801−12816.
(37) Harrison, A. W.; Ryazanov, M.; Sullivan, E.; Neumark, D. M. Photodissociation Dynamics of the Methyl Perthiyl Radical at 248 and 193 nm. Manuscript in preparation.
(38) Continetti, R. E.; Cyr, D. R.; Metz, R. B.; Neumark, D. M. Fast Beam Studies of N_3 Photodissociation. *Chem. Phys. Lett.* **1991**, *182*, 406−411.
(39) Continetti, R. E.; Cyr, D. R.; Osborn, D. L.; Leahy, D. J.; Neumark, D. M. Photodissociation Dynamics Of the N_3 Radical. *J. Chem. Phys.* **1993**, *99*, 2616−2631.
(40) Shapero, M.; Cole-Filipiak, N. C.; Haibach-Morris, C.; Neumark, D. M. Benzyl Radical Photodissociation Dynamics at 248 nm. *J. Phys. Chem. A* **2015**, *119*, 12349.
(41) Lee, Y. T.; McDonald, J. D.; LeBreton, P. R.; Herschbach, D. R. Molecular Beam Reactive Scattering Apparatus with Electron Bombardment Detector. *Rev. Sci. Instrum.* **1969**, *40*, 1402−1408.
(42) Robinson, J. C.; Harris, S. A.; Sun, W.; Sveum, N. E.; Neumark, D. M. Photofragment Translational Spectroscopy of 1,3-Butadiene and 1,3-Butadiene-1,1,4,4-d^4 at 193 nm. *J. Am. Chem. Soc.* **2002**, *124*, 10211−10224.
(43) Kohn, D. W.; Clauberg, H.; Chen, P. Flash Pyrolysis Nozzle for Generation of Radicals in a Supersonic Jet Expansion. *Rev. Sci. Instrum.* **1992**, *63*, 4003−4005.
(44) Negru, B.; Just, G. M. P.; Park, D.; Neumark, D. M. Photodissociation Dynamics of the *tert*-Butyl Radical via Photofragment Translational Spectroscopy at 248 nm. *Phys. Chem. Chem. Phys.* **2011**, *13*, 8180−8185.
(45) Cole-Filipiak, N. C.; Shapero, M.; Negru, B.; Neumark, D. M. Revisiting the Photodissociation Dynamics of the Phenyl Radical. *J. Chem. Phys.* **2014**, *141*, 104307.
(46) Benson, S. W. Thermochemistry and Kinetics of Sulfur-Containing Molecules and Radicals. *Chem. Rev.* **1978**, *78*, 23−35.
(47) Kuhnke, K.; Kern, K.; David, R.; Comsa, G. High Efficiency Molecular-Beam Ionization Detector with Short Ionization Region. *Rev. Sci. Instrum.* **1994**, *65*, 3458−3465.
(48) Casavecchia, P.; Leonori, F.; Balucani, N.; Petrucci, R.; Capozza, G.; Segoloni, E. Probing the Dynamics of Polyatomic Multichannel Elementary Reactions by Crossed Molecular Beam Experiments with Soft Electron-Ionization Mass Spectrometric Detection. *Phys. Chem. Chem. Phys.* **2009**, *11*, 46−65.
(49) Daly, N. R. Scintillation Type Mass Spectrometer Ion Detector. *Rev. Sci. Instrum.* **1960**, *31*, 264−267.
(50) Butler, L. J.; Hintsa, E. J.; Shane, S. F.; Lee, Y. T. The Electronic State-Selective Photodissociation of CH_2BrI at 248, 210, and 193 nm. *J. Chem. Phys.* **1987**, *86*, 2051−2074.
(51) Mueller, J. A.; Morton, M. L.; Curry, S. L.; Abbatt, J. P. D.; Butler, L. J. Intersystem Crossing and Nonadiabatic Product Channels in the Photodissociation of N_2O_4 at 193 nm. *J. Phys. Chem. A* **2000**, *104*, 4825−4832.
(52) Hobrock, B. G.; Kiser, R. W. Electron Impact Investigations of Sulfur Compounds. III. 2-Thiapropane, 3-Thiapentane, 2,3,4-Trithiapentane. *J. Phys. Chem.* **1963**, *67*, 1283−1286.
(53) Lias, S. G.; Bartmess, J. E.; Liebman, J. F.; Holmes, J. L.; Levin, R. D.; Mallard, W. G. Ion Energetics Data. In *NIST Chemistry WebBook*; NIST Standard Reference Database Number 69; National Institute of Standards and Technology: Gaithersburg, MD 20899.
(54) Field, F. H.; Franklin, J. L. *Electron Impact Phenomena and the Properties of Gaseous Ions*; Academic Press, Inc.: New York, 1957.
(55) Matt, S.; Echt, O.; Wörgötter, R.; Grill, V.; Scheier, P.; Lifshitz, C.; Märk, T. D. Appearance and Ionization Energies of Multiply-Charged C_{70} Parent Ions Produced by Electron Impact Ionization. *Chem. Phys. Lett.* **1997**, *264*, 149−156.
(56) NIST: Electron-Impact Cross Section Database. http://www.nist.gov/pml/data/ionization/index.cfm (accessed October 20, 2015).
(57) Baiocchi, F. A.; Wetzel, R. C.; Freund, R. S. Electron-Impact Ionization and Dissociative Ionization of the CD_3 and CD_2 Free Radicals. *Phys. Rev. Lett.* **1984**, *53*, 771−774.
(58) Zare, R. N. Photoejection Dynamics. *Mol. Photochem.* **1972**, *4*, 1−37.
(59) Harich, S. A. PHOTRAN, A Program for Forward Convolution Analysis of Photodissociation, 2003.
(60) Henri, V.; Teves, M. C. Absorption Spectrum and Constitution of Sulphur Vapour. Predissociation of Molecules. *Nature* **1924**, *114*, 894.

DOI: 10.1021/acs.jpca.5b12284
J. Phys. Chem. A XXXX, XXX, XXX−XXX

(61) Anastasi, C.; Broomfield, M.; Nielsen, O. J.; Pagsberg, P. Ultraviolet Absorption Spectra and Kinetics of CH_3S and CH_2SH Radicals. *Chem. Phys. Lett.* **1991**, *182*, 643−648.
(62) Price, W. C.; Simpson, D. M. The Absorption Spectra of Sulphur Dioxide and Carbon Disulphide in the Vacuum Ultra-Violet. *Proc. R. Soc. London, Ser. A* **1938**, *165*, 272−291.
(63) Walsh, A. D. The Electronic Orbitals, Shapes, and Spectra of Polyatomic Molecules. Part II. Non-Hydride AB_2 and BAC Molecules. *J. Chem. Soc.* **1953**, 2266−2288.
(64) Krajnovich, D.; Huisken, F.; Zhang, Z.; Shen, Y. R.; Lee, Y. T. Competition Between Atomic and Molecular Chlorine Elimination in the Infrared Multiphoton Dissociation of CF_2Cl_2. *J. Chem. Phys.* **1982**, *77*, 5977−5989.
(65) Hwang, W.; Kim, Y.-K.; Rudd, M. E. New Model for Electron-Impact Ionization Cross Sections of Molecules. *J. Chem. Phys.* **1996**, *104*, 2956−2966.
(66) Shao, Y.; Gan, Z.; Epifanovsky, E.; Gilbert, A. T. B.; Wormit, M.; Kussmann, J.; Lange, A. W.; Behn, A.; Deng, J.; Feng, X.; et al. Advances in Molecular Quantum Chemistry Contained in the Q-Chem 4 Program Package. *Mol. Phys.* **2015**, *113*, 184−215.
(67) Negru, B.; Goncher, S. J.; Brunsvold, A. L.; Just, G. M. P.; Park, D.; Neumark, D. M. Photodissociation Dynamics of the Phenyl Radical via Photofragment Translational Spectroscopy. *J. Chem. Phys.* **2010**, *133*, 074302.
(68) Jonah, C. Effect of Rotation and Thermal Velocity on the Anisotropy in Photodissociation Spectroscopy. *J. Chem. Phys.* **1971**, *55*, 1915−1922.

DOI: 10.1021/acs.jpca.5b12284
J. Phys. Chem. A XXXX, XXX, XXX−XXX